General Disclaimer

One or more of the Following Statements may affect this Document

- This document has been reproduced from the best copy furnished by the organizational source. It is being released in the interest of making available as much information as possible.

- This document may contain data, which exceeds the sheet parameters. It was furnished in this condition by the organizational source and is the best copy available.

- This document may contain tone-on-tone or color graphs, charts and/or pictures, which have been reproduced in black and white.

- This document is paginated as submitted by the original source.

- Portions of this document are not fully legible due to the historical nature of some of the material. However, it is the best reproduction available from the original submission.

NASA Technical Memorandum 79145

IDENTIFICATION AND DUAL ADAPTIVE CONTROL OF A TURBOJET ENGINE

Walter Merrill
Lewis Research Center
Cleveland, Ohio

and

Gary Leininger
University of Toledo
Toledo, Ohio

Prepared for the
Fifth IFAC Symposium on Identification and System Parameter Estimation
Darmstadt, Federal Republic of Germany, September 24-28, 1979

IDENTIFICATION AND DUAL ADAPTIVE CONTROL OF A TURBOJET ENGINE

Walter Merrill

National Aeronautics and Space Administration
Lewis Research Center
Cleveland, Ohio, U.S.A.

and

Gary Leininger

University of Toledo
Toledo, Ohio, U.S.A.

Abstract. The objective of this paper is to utilize the design methods of modern control theory to realize a "dual-adaptive" feedback control unit for a highly non-linear single spool airbreathing turbojet engine.

Using a very detailed and accurate simulation of the non-linear engine as the data source, linear operating point models of unspecified dimension are identified. Feedback control laws are designed at each operating point for a prespecified set of sampling rates using sampled-data output regulator theory.

The control system sampling rate is determined by an adaptive sampling algorithm in correspondence with turbojet engine performance. The result is a "dual-adaptive" control law that is functionally dependent upon the sampling rate selected and environmental operating conditions. Simulation transients demonstrate the utility of the dual-adaptive design to improve on-board computer utilization while maintaining acceptable levels of engine performance.

I. INTRODUCTION

To generate required propulsive thrust levels and maintain structural and thermodynamic engine integrity, control system designs for gas turbine engines of the past several decades only required the proper manipulation of engine fuel flow (and possibly fan nozzle area). Control objectives emphasized component reliability and design simplicity to maintain operating performance specifications. However, recent aircraft operational requirements such as those imposed for supersonic flight, VTOL capability and improved fuel conservation dictate the development of gas turbine engines with increased performance capabilities over an expanded operating environment. Consequently, turbofan engine control designs to meet these performance demand schedules will require significant increases in control flexibility. This increase in flexibility may assume the form of extensive variable geometries, variable pitch fan blades and/or the utilization of digital computers for engine performance evaluation and control.

In this paper, we assume the presence of an on-board digital computer to perform system management tasks which include the monitoring and control of turbofan engine performance. In this regard, the computer may not be totally dedicated to engine control except perhaps during critical operating periods. Thus the data monitoring and control sampling rates may vary in correspondence with the operating conditions and performance requirements of the overall aircraft system.

From an engine control viewpoint, the sampling rate and feedback gains are integrally related if operating point engine performance is to be maintained at acceptable levels. To allow for this degree of flexibility in engine control, linear models (at each operating point) for a preselected set of sampling rates need to be identified. Once the models are known, feedback control laws can be obtained using sampled-data output regulator theory. The engine control system sampling rate at a particular operating point is then determined by an adaptive sampling algorithm in correspondence with turbojet engine performance. Repeating this procedure for several operating conditions results in a "dual-adaptive" control law that is functionally dependent upon the sampling rate selected and the environmental operating conditions.

In the next section, the Tse and Weinert [1] method is used to identify model order and structure for several operating point models of a turbojet engine over a finite set of system sampling rates. The models are used in Section III to develop a dual adaptive control configuration. In Section IV the results of a dual adaptive control design for a turbojet engine are discussed.

II. ENGINE MODEL IDENTIFICATION

Previous work in identifying gas turbofan engine models has been done by Otto and Taylor [2], Crooks and Willshire [3], Ahlbeck [4], Chen [5], Michael and Farrar [6] and Mueller [7]. These techniques assume a model order to obtain linear models from transfer function data [4,5,7] or by least square curve fitting procedures [6]. In [6] the least squares method in [6] was combined with a dynamic non-linear filter to identify gas turbine dynamics from stochastic input output data. Using a perturbational method with an output error evaluation procedure, DeHoff and Hall [9] obtain an iterative equation from a synthesized time derivative of the state vector to identify system order [10]. Although these methods are suitable for hydromechanical control designs, most are not extendable to the digital control format established in the previous section. For this purpose the Tse and Weinert method is selected.

Using output data, the Tse and Weinert method identifies a constant, multivariable, stochastic linear system which has unknown dimension, matrix parameters and noise covariances. Since the output data set determine an equivalence class of systems [1], a general stochastic system model cannot be identified from steady state output data alone. However, each system model in this equivalence class has a steady state Kalman filter with a common impulse response and innovations covariance [11]. If the system matrices are chosen in a certain unique cononical form, consistant Kalman filter parameter estimates can be obtained. Thus through the identification of the Kalman filter model for the equivalence class, a state model for the unknown system can be obtained.

Using the notation in [1], the steady-state Kalman filter for the equivalence class is given by

$$\begin{aligned} z_{k+1} &= A\, z_k + K\, u_k \\ y_k &= C\, z_k + u_k \end{aligned} \tag{1}$$

where z_k is an n vector, y_k is an m vector, the Gaussian innovations process u_k has unknown covariance

$$E\{u_i, u_j\} = Q\, \delta_{ij}$$

and K is the Kalman gain matrix. The unknown vector $\theta_1 = \{A,C,K,Q\}$ in addition to the model order n^1 is identifiable if (1) A is stable, (2) the set (A,K,C) is a minimal realization and (3) the specific cononical structure for A (as given in [1]) is used.

With $Y^N = \{y_k\}_{k=1}^N$ as the observed data set, time series analysis can be used to approximate the output covariance R(σ) using

$$\hat{R}(\sigma) = \frac{1}{N} \sum_{i=1}^{N-\sigma} y(i+\sigma)\, y^T(i) \tag{2}$$

Forming the identifiability matrix

$$\phi_i^j(\gamma) = \begin{bmatrix} \hat{r}_{ij}(1) & - - - & \hat{r}_{ij}(\gamma) \\ \hat{r}_{ij}(2) & & \hat{r}_{ij}(\gamma+1) \\ \vdots & & \vdots \\ \hat{r}_{ij}(\gamma) & - - - & \hat{r}_{ij}(2\gamma-1) \end{bmatrix} \tag{3}$$

and defining

$$d_i^j(\gamma) = \mathrm{DET}\,\{\phi_i^j(\gamma)\} \tag{4}$$

the index γ is then incremented until $d_i^j(\gamma^*)=0$. Set $p_i = \gamma^*-1$ which represents the smallest non-negative integer such that row i of the observability matrix (A,C) is linearly dependent on the vectors in all preceeding rows. Since

$$\sum_{i=1}^{m} p_i = n \tag{5}$$

where m is the number of output variables, the unknown system order, n, can be determined. Following [1, 12] the elements in A and C can be determined from (2), (3) and p_i in (5) [1].

This identification method was applied to stochastic data obtained from an accurate non-linear digital simulation of a turbojet engine [13]. The simulation incorporates a real gas combustion model and experimentally determined compressor and turbine data. Dynamics are represented by formal one-dimensional inviscid continuity, momentum and energy approximations to unsteady compressor, combustor and exhaust nozzle conditions. The simulation represents a single rotor turbojet with each steady-state operation point uniquely determined by rotor speed, S, flight mach number, M, and flight altitude, η.

Eight engine variables (m=8) were selected as system outputs: rotor speed (S), compressor discharge temperature (T_c) and pressure (P_c), nozzle inlet temperature (T_z) and pressure (P_z), turbine inlet temperature (T_T) and pressure (P_T), and engine thrust (F). For this study the engine input is fuel flow, ω_f.

The engine is modeled as

$$\begin{aligned} \dot{x} &= f(x, \omega_f, S) + \zeta(t) \\ y(t) &= g(x, \omega_f, S) + \eta(t) \end{aligned} \tag{6}$$

where $x \in R^n$ and $y \in R^8$. The sampled-data linearized operating point model for (6) is given by

$$\begin{aligned} \delta x_{k+1} &= A\, \delta x_k + B\, \delta\omega_f + \zeta_k \\ \delta y_k &= C\, \delta x_k + D\, \delta\omega_f + \eta_k \end{aligned} \tag{7}$$

where A, B, C, D, model order n and noise covariances are unknown.

Data for the identification method was obtained from the non-linear simulation over a fifteen second interval (after steady state conditions were achieved) by perturbing the system via

ω_f with white noise. Designating the engine rotor speed of 36, 960 rpm as the 100% operating point, four operating points corresponding to 80%, 90%, 100% and 104.5% rotor speed were selected. The 80% and 104.5% operating points correspond to minimum and maximum rotor design speeds, respectively. Typical data histories for S and T_T are shown in Fig. 1.

Following the procedure outlined above, $\hat{R}(\sigma)$ was calculated at each operating point using the appropriate δY^N data set. The identifiability matrix was formed from $\hat{R}(\sigma)$ with $d_i^j(\gamma)$ in (4) subsequently evaluated. Figure 2 indicates $d_i^j(\gamma)$ as γ varies when j=1 (rotor speed) and j=6 (turbine temperature). Using a structure criterion $\varepsilon = 0.1$, it follows from Fig. 2 that $p_1 = 2$. Evaluating (3) and (4) for i=2,3,...,8 yields $\{p_i\}_{i=2}^{m} = \{0\}$ and suggests that each output for $i \geq 2$ is a linear combination of the two state variables associated with p_1. Thus from (5), n = 2.

The system matrices A and C were subsequently evaluated at each operating point and appear in Table 1. To complete the model in (7), B and D were identified using a gradient search procedure. With n = 2 and m = 8, the ten unknown elements were obtained using a sum of squared errors cost function for gradient evaluation over a five second transient. The test input in each case was

$$\delta\omega_f(k) = \Lambda \sum_{q=1}^{3} \text{Sin}\,(\omega_q k + \psi_q) \qquad (8)$$

with ψ_1=.1, ψ_2=0, ψ_3=1.0, ω_1=.2, ω_2=2 and ω_3=20. The input magnitude, Λ, was adjusted to limit perturbations to the linear region about each operating point. Table 2 indicates the matrices B and D obtained for each operating point.

The identification results were verified using the fuel flow test input of Fig. 3. The input is a combination step, ramp and parabola large enough to drive the engine operating point from 85% to 100% speed and was applied to the non-linear simulation and the composite model of Fig. 4. The composite model was generated by scheduling the identified A, B, C and D matrices as a function of rotor speed, S. Linear interpolation was used to obtain dynamics between identified operating point models. Trajectory comparisons for S and T_T are given in Figs. 5 and 6. Discrepancies in the figures are attributed to the high frequency content in T_T and T_2 (not shown) and to the limited spectrum of the model (approximately 5 Hz.)

In the next section, the identified operating point models are used to obtain constant output feedback gain matrices at each operating point.

III. DUAL ADAPTIVE CONTROL

Adaptive sampling varies the sampling rate T as a function of a system parameter to improve computer utilization and sampling efficiency. Here sampling efficiency is defined as the ratio of system performance to the number of samples required to achieve that performance, i.e.,

$$\eta_A = \frac{1}{J_A N_A} \qquad (9)$$

where J_A is the value of the cost function (inverse of performance) and N_A is the number of samples. As N_A decreases for constant J_A, η_A increases, thereby improving computer utilization.

Using (9) as a general guide, the adaptive sampling law [14] used in the turbojet application [12] is

$$T_k = \begin{cases} T_1 & T_{min} \leq T_1 \leq T_{max} \\ T_{min} & T_1 \leq T_{min} \\ T_{max} & T_1 \geq T_{max} \end{cases} \qquad (10)$$

where

$$T_1 = \frac{T_{max}}{\alpha\,[e_k]^2 + 1} \qquad (11)$$

T_{min} and T_{max} are lower and upper bounds on the sampling rate respectively. The variable e_k was selected as

$$e_k = \frac{S_k - S_{k-1}}{T_{k-1}\,S_{k-1}} \qquad (12)$$

where S_k is engine core speed. Core speed was selected since it is readily measurable and a good indicator of dynamic engine performance. Sampling limits were established as

$$T_{min} = .001 \text{ sec.}$$

$$T_{max} = .025 \text{ sec.}$$

The variable α in (11) reflects the relative weighting between sampling cost (efficiency) and the squared error cost due to sampling. For the application in this paper $\alpha = 4(10^4)$.

For a constant sampling rate the corresponding sampled-data system and steady-state feedback gain matrix obtained from discrete output feedback regulator theory [12] is time-invariant. With adaptive sampling, the corresponding sampled-data system is functionally dependent on T_k and therefore will be time-varying even though the original continuous process is time-invariant. If T_k were known for all k over the interval of control, the time evolution of the discrete system would be known and the feedback gain matrix could be obtained from the time-varying regulator equations. However, $\{T_k\}$ is not known a priori but is a function of a system parameter and will vary with engine performance and environment. Thus the feedback gain matrix cannot be determined

in the usual way since T_k at future sampling instants is not available. To overcome this difficulty, it is assumed that T_k determined at instant k will be sustained for all future time instants. With this assumption, a feedback control matrix can be computed using steady state discrete optimal feedback regulator theory. Now, feedback gains can be computed off-line for a sufficient number of sampling periods to establish a functional relationship between system gains and T. This relationship can easily be stored in a digital computer memory and used on-line to generate the control input to the continuous process.

As the system progresses through the operating range, the functional gain relationship becomes dependent upon the operating point conditions as well as the sampling interval. Thus the dual adaptive nature of the control is created.

IV. APPLICATION [12]

In this section the dual adaptive control of Section III is applied to the operating point models obtained in Section II.

Case 1 $y(t) = S$

The control task is to accelerate the engine from steady-state at 90% to steady-state at 100% rotor speed. The sampling rate was held constant at T_{min} with regulator weighting matrices selected as Q=10 and R=1. The resultant cost function J_ω is then used to evaluate sampling efficiency $\eta=1/J_\omega N_f$ and provides a baseline comparison for the remaining cases (see Table 3).

Case 2 $y(t) = S$

Adaptive sampling was incorporated into the control configuration of case 1. The results show approximately a 10% increase in J_ω and a 100% improvement in sampling efficiency with no visible differences in the time plots.

Case 3 $y(t) = S$

To examine the effect of a change in the weighting coefficients of case 2, set Q=50 and retain R=1. The results are plotted with those of case 2 in Figs. 7 - 10. Case 3 control, as expected, accelerates the engine faster than the case 2 control. Rotor speed is within 1% of steady state in 0.6 sec. and the thrust acceleration rise time is 0.4 sec. as compared to 1.1 sec. and 1.2 sec. for case 2 respectively. The penalty for this improved acceleration of case 3 is higher turbine inlet temperature and additional fuel flow requirements.

Case 4

To evaluate the ability of the adaptive digital control to limit turbine temperature, assume a temperature limit for the turbojet of 1900°R. The control configuration must now accelerate the engine from 90% to 104.5% design speed without violating the 1900°R constraint.

This temperature constrained acceleration is accomplished by initially controlling the engine as in case 2 with $y(t) = S$ until the 1900°R limit is exceeded. Then the control configuration is changed to include both rotor speed, S, and T_T feedback, i.e., $y(t) = [S \quad T_T]^T$, with Q=diag [.1, .0001] and R=1. Once the temperature constraint is satisfied, the control reverts to the original case 2 feedback arrangement. The results are documented in Table 3 and are plotted with those of case 2 in Figs. 11 - 13.

V. CONCLUSIONS

System model identification, discrete optimal output regulator feedback and adaptive sampling methods were combined to develop a dual adaptive control technique. This technique was applied to a non-linear turbojet engine to obtain a feedback control over multi-operating point conditions. The example application clearly demonstrates the utility of the design approach.

VI. ACKNOWLEDGEMENTS

This research was supported in part by the National Aeronautics and Space Administration-Lewis Research Center under NASA grant NGR-36-010-024.

VII. REFERENCES

1. Tse, E. and H. Weinert (October 1975). Structure determination and parameter identification for multivariable stochastic linear systems. IEEE Transactions on Automatic Control, AC-20, No. 5.

2. Otto, E. and B. Taylor (1951). Dynamics of a turbojet considered as a Quasi-static system. NACA Report No. R1001.

3. Crooks, P. and Willshire (1956). The theoretical estimation of engine speed response data for a turbojet engine. NGTE Report No. M268.

4. Ahlbeck, D. (1966). Simulation. Vol. 7.

5. Chen, C. (1972). Model reduction of multivariable control systems. Fifth IFAC World Congress.

6. Michael, G. and F. Farrar (1973). Development of optimal control modes for advanced technology propulsion systems. UARL Report No. M9-1160-1.

7. Mueller, G. (1971). Linear model of a 2-shaft turbojet and its properties. Proc. IEE, 118, No. 6.

8. Michael, G. and F. Farrar (March 1975). Identification of multivariable gas turbine

dynamics from stochastic input-output data. ONR TR-R941620-3, Contract No. N00014-73-C-0281.

9. DeHoff, R. L. and W. E. Hall (June 1977). System identification principles applied to multivariable control of the F100 turbojet engine. 1977 JACC, San Francisco.

10. Gupta, N. K. and W. E. Hall (February 1976). Model structure determination and test input selection for identification of nonlinear regimes. System Control Inc., ONR Contract Report CR-215-213-5.

11. Tse, E. and J. Anton (October 1972). On the identifiability of parameters. IEEE Trans. Autom. Control, AC-17.

12. Merrill, W. C. (May 1975). An application of modern control theory to jet propulsion systems. Ph.D. Dissertation, University of Toledo, May 1975; also NASA TMX-71726.

13. Seldner, K., L. C. Geyser, H. Gold, D. Walker and G. Burgner (1972). Performance and control study of a low pressure ratio turbojet engine for a drone aircraft. NASA TMX-2537.

14. Hsia, T. (February 1974). Analytic design of adaptive sampling control laws in sampled-data systems. IEEE Trans. Autom. Control, AC-19, No. 1.

TABLE 1 Identified Values of A and C vs. % Speed-Discrete Model

% Speed	Matrix	Matrix Elements						
80	A	0 -.354	1 1.233					
	C^T	1 0	.0127 -.00046	.0019 -.00009	-.0338 .00418	.00029 -.00002	-.028 .0035	.0016 -.00011	.018 -.0012
90	A	0 -.340	1 1.183					
	C^T	1 0	.0144 -.00069	.0023 -.00017	-.0264 .00380	.00089 -.00004	-.023 .0037	.0021 -.00017	.023 -.0023
100	A	0 -.258	1 1.060					
	C^T	1 0	.0153 -.00064	.0025 -.00020	-.0200 .00366	.00051 -.00006	-.017 .0038	.0023 -.00023	.026 -.0034
104.5	A	0 -.318	1 1.119					
	C^T	1 0	.0163 -.0013	.0027 -.00049	-.018 .0047	.00053 -.00008	-.016 .0036	.0025 -.00034	.028 -.0044

TABLE 2 Identified Values of B and D vs. % Speed

% Speed	Matrix	Matrix Elements							
80	B^T	48004.7	27815.9						
	D^T	-12227.78	-15.25	12.47	3508.81	2.598	3991.66	13.96	-11703.98
90	B^T	43653.5	24165.8						
	D^T	-10573.77	-33.38	4.550	2920.50	2.970	3427.02	9.0856	114.41
100	B^T	45947.6	19977.63						
	D^T	-18929.90	-223.59	-26.322	2535.71	-.9140	2870.89	-23.637	-117.678
104.5	B^T	40617.6	19662.8						
	D^T	-14468.60	-203.73	-19.96	2299.11	.5885	2632.15	-20.069	-43.53

TABLE 3 Summary of Simulation Results

Simulation Test	Weighting Matrices Q, R	Number of Samples, N_f	Regulator Performance Index, J_ω	Sampling Efficiency, η
Case 1	10, 1	1928	.00315	.1650
Case 2	10, 1	878	.00337	.3380
Case 3	50, 1	621	.0256	.0628
Case 4	10, 1	900	.00279	.3980

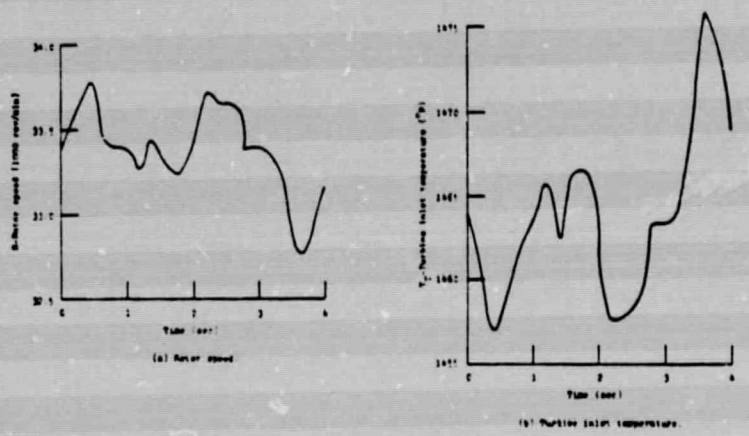

Fig. 1. Typical output trajectories for a Gaussian Disturbance.

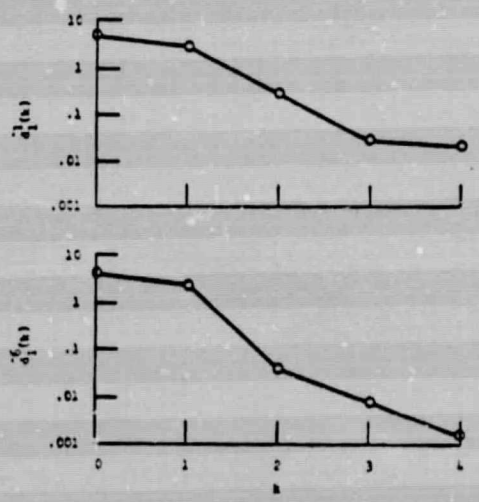

Fig. 2. $d_i^j(k)$ vs. k for i=1 and j=1, 6.

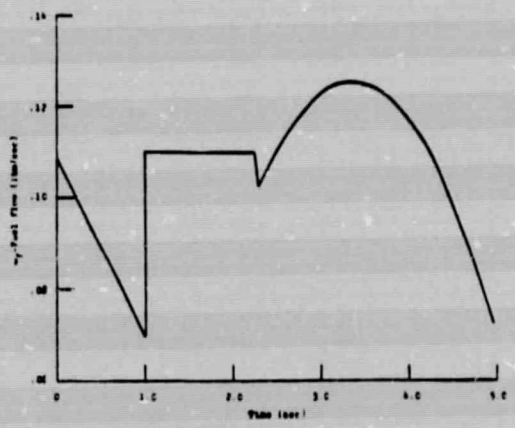

Fig. 3. The test input.

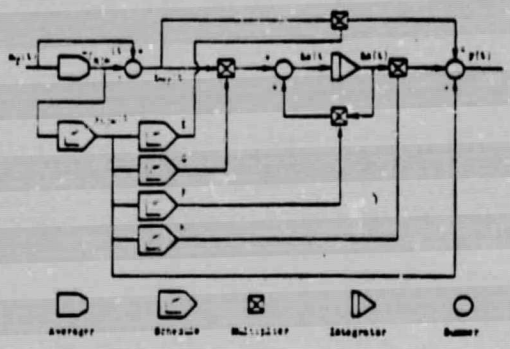

Fig. 4. Composite engine.

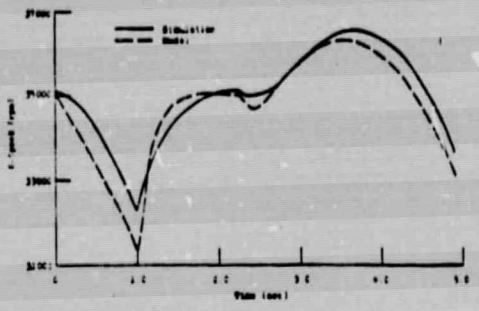

Fig. 5. Rotor Speed for simulation and composite model.

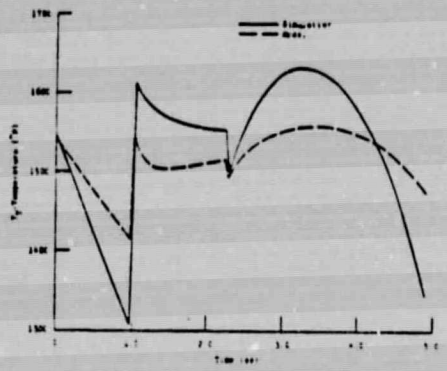

Fig. 6. Turbine Inlet Temperature for simulation and composite model.

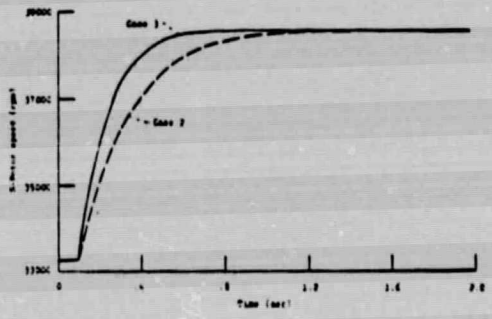

Fig. 7. Case 2 and Case 3 engine accelerations - Rotor Speed.

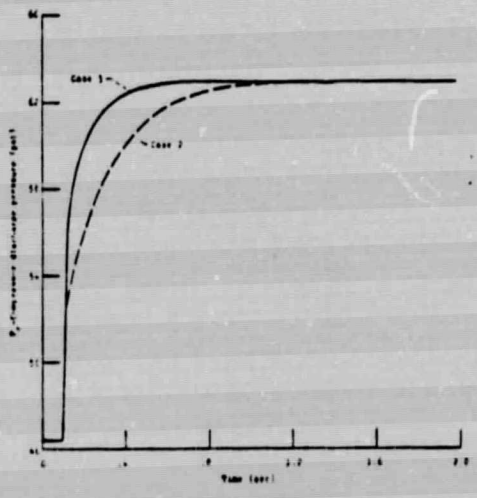

Fig. 8. Case 2 and Case 3 engine accelerations - Compressor Discharge Pressure.

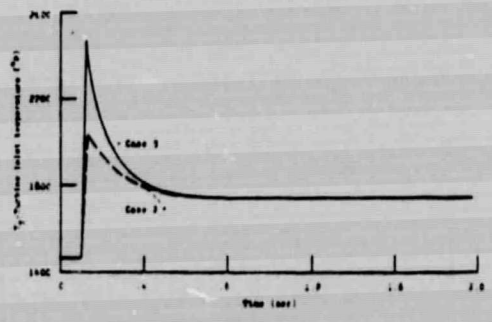

Fig. 9. Case 2 and Case 3 engine accelerations - Turbine Temperature.

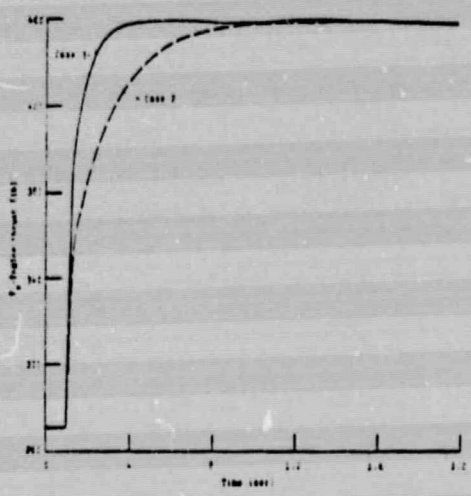

Fig. 10. Case 2 and Case 3 engine accelerations - Thrust.

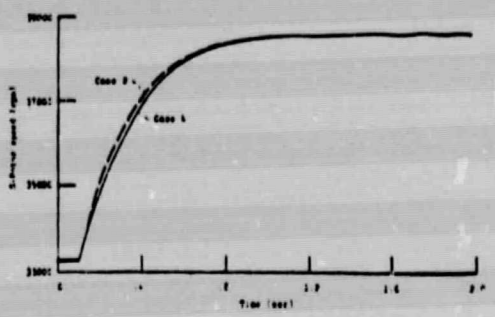

Fig. 11. Case 4 and Case 2 accelerations - Rotor Speed.

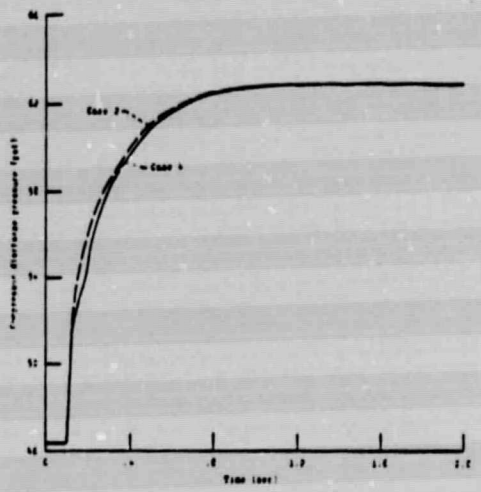

Fig. 12. Case 4 and Case 2 engine accelerations - Compressor Discharge Pressure.

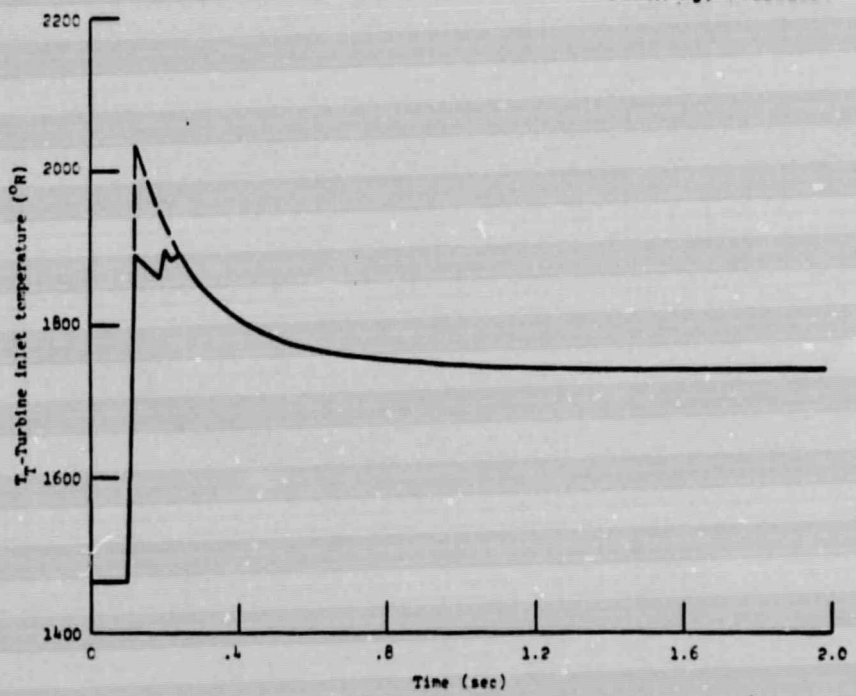

Fig. 13. Case 4 and Case 2 engine accelerations for Turbine Temperature.